



## Hydrogenation of succinic acid to 1,4-butanediol over Re–Ru bimetallic catalysts supported on mesoporous carbon

Ki Hyuk Kang, Ung Gi Hong, Yongju Bang, Jung Ho Choi, Jeong Kwon Kim, Jong Kwon Lee, Seung Ju Han, In Kyu Song\*

School of Chemical and Biological Engineering, Institute of Chemical Processes, Seoul National University, Shinlim-dong, Kwanak-ku, Seoul 151-744, South Korea



### ARTICLE INFO

#### Article history:

Received 10 September 2014

Received in revised form

17 November 2014

Accepted 20 November 2014

Available online 26 November 2014

#### Keywords:

Hydrogenation

Succinic acid

1,4-Butanediol

Bimetallic catalyst

Re–Ru catalyst

### ABSTRACT

A series of Re–Ru bimetallic catalysts supported on mesoporous carbon (denoted as  $(0.6 - x)\text{Re}-x\text{Ru}/\text{MC}$ ) were prepared by a single-step surfactant-templating method and a subsequent incipient wetness impregnation method with a variation of ruthenium loading ( $x$ , mol%), and they were applied to the liquid-phase hydrogenation of succinic acid to 1,4-butanediol (BDO). The effect of metal content on the catalytic activities and physicochemical properties of  $(0.6 - x)\text{Re}-x\text{Ru}/\text{MC}$  catalysts was investigated. It was found that a Re–Ru miscible phase was formed in the catalysts during the reduction process, and it was responsible for strong interaction between rhenium and ruthenium. It was also revealed that reducibility, metal dispersion, and oxidation state of  $(0.6 - x)\text{Re}-x\text{Ru}/\text{MC}$  catalysts were affected by Re:Ru molar ratio. In particular, the oxidation state was closely related to the hydrogen adsorption behavior of the catalysts. The amount of weak hydrogen-binding sites increased with increasing the ratios of metallic rhenium ( $\text{Re}^0$ ) and ruthenium ( $\text{Ru}^0$ ) with respect to total metallic species in the reduced  $(0.6 - x)\text{Re}-x\text{Ru}/\text{MC}$  catalysts. Catalytic performance in the hydrogenation of succinic acid to BDO over  $(0.6 - x)\text{Re}-x\text{Ru}/\text{MC}$  showed a volcano-shaped trend with respect to Re:Ru molar ratio. This result was well correlated with the amount of weak hydrogen-binding sites of the catalysts. Among the catalysts tested,  $0.3\text{Re}-0.3\text{Ru}/\text{MC}$  with the largest amount of weak hydrogen-binding sites showed the best catalytic performance in the BDO production by hydrogenation of succinic acid.

© 2014 Elsevier B.V. All rights reserved.

## 1. Introduction

1,4-Butanediol (BDO) is a versatile chemical that can be used in a wide range of industrial applications. BDO has been used as an organic solvent and a fine chemical for production of adhesives, fibers, and polyurethanes [1–4]. Recently, BDO has received much attention as an important raw material for thermoplastic polymers such as polybutylene succinate (PBS) and polybutylene terephthalate (PBT) [5]. As the consumption of these polymers is growing faster in electronics and automobile industries, in particular, the global demand for BDO is expected to increase rapidly.

BDO has been produced through several conventional routes: hydrogenation of maleic anhydride [6], isomerization of propylene oxide [6], and acetoxylation of butadiene [4]. These processes rely on petrochemical feedstocks derived from fossil fuel. Due to the limited amount of fossil fuel, however, current research trend for

BDO production moves toward the utilization of renewable energy sources such as biomass. In this respect, conversion of succinic acid to BDO by catalytic hydrogenation has attracted recent attraction as a promising process, because succinic acid can be obtained from bio-refinery process [5].

Hydrogenation of succinic acid to BDO occurs via two-step hydrogenation reactions as shown in Fig. 1. Succinic acid is first transformed into  $\gamma$ -butyrolactone (GBL) by hydrogenation, and then BDO or tetrahydrofuran (THF) is formed through consecutive hydrogenation of GBL [4]. For the catalytic conversion of succinic acid, various noble metal catalysts such as Pd [7–9], Pt [10], Rh [10], Ru [11,12], and Re [13] have been investigated. Among these catalysts, rhenium has been considered as the most efficient monometallic catalyst for the selective formation of BDO. However, several studies have shown that rhenium alone was not sufficient to obtain high yield for BDO [5,14–17].

In an attempt to improve BDO production by hydrogenation of succinic acid, Re-based bimetallic catalysts, including Re–Pt/C [14], Re–Pd/C [14,15], Re–Pd/TiO<sub>2</sub> [16], and Re–Ru/C [15,17], have been investigated. Nonetheless, the researches have rarely elucidated

\* Corresponding author. Tel.: +82 2 880 9227; fax: +82 2 889 7415.

E-mail address: [inksong@snu.ac.kr](mailto:inksong@snu.ac.kr) (I.K. Song).

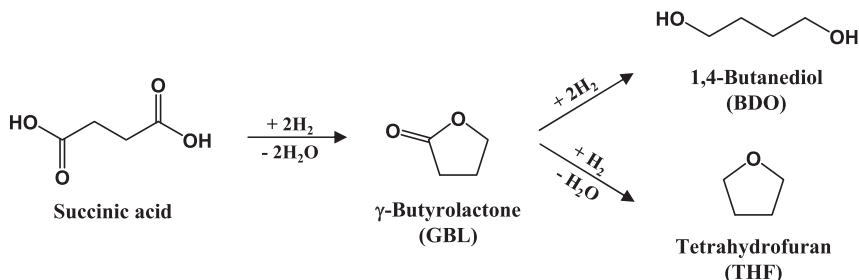


**Fig. 1.** Reaction pathways for hydrogenation of succinic acid.

the effect of interaction between rhenium and other metal on the selective formation of BDO from succinic acid. This is because combination of rhenium and noble metal causes difficulty in structural and chemical analyses. For example, rhenium can be miscible with noble metals such as Pt, Pd, and Ru to form a solid-solution due to their similar atomic sizes and surface energies [18–20], which complicates characterization. Moreover, since rhenium does not cause dissociative hydrogen chemisorption at low temperature [21,22], either modified hydrogen chemisorption or CO chemisorption method is essential for determining metal dispersion of Re-based catalyst. In this respect, a systematic investigation on the effect of interaction between rhenium and other metal on the catalytic activities and physicochemical properties of Re-based bimetallic catalyst would be worthwhile.

In this work, a series of Re–Ru bimetallic catalysts with different metal content were supported on mesoporous carbon, and they were applied to the liquid-phase hydrogenation of succinic acid to BDO. The effect of metal content on the catalytic activities and physicochemical properties of the catalysts was investigated. The catalysts were characterized by nitrogen adsorption–desorption, TPR, XRD, CO chemisorption, TEM, STEM-EDX mapping, XPS, and H<sub>2</sub>-TPD analyses.

## 2. Experimental

### 2.1. Preparation of (0.6 – x)Re–xRu/MC catalysts

A series of Re–Ru bimetallic catalysts supported on mesoporous carbon were prepared by a single-step surfactant-templating method and a subsequent incipient wetness impregnation method. For the preparation of mesoporous carbon (MC), 5 g of P123 copolymer (Sigma–Aldrich) was dissolved in deionized water (130 ml) at room temperature under vigorous stirring. 2.1 g of sucrose (Sigma–Aldrich) as a carbon precursor and 20 ml of HCl solution (35%) were then added into the solution. Subsequently, 1.9 ml of H<sub>2</sub>SO<sub>4</sub> solution (95%) was added into the solution to promote later cross-linkage of P123 with tetraethoxysilane (TEOS). After maintaining the solution with stirring for 1 h, 9.3 ml of TEOS (Sigma–Aldrich) as a structure-directing agent was slowly added into the mixed solution. The resulting solution was stirred at 37 °C for 24 h, and it was then kept at 100 °C for 24 h without stirring for self-assembly of micelle structure. The resultant was dried at 100 °C for 48 h, and then carbonized at 800 °C for 4 h at a heating rate of 5 °C/min in a nitrogen stream (50 ml/min). The obtained carbon–silica composite was then treated with 300 ml of HF solution (5%) for 24 h to remove silica template, and it was finally filtered and dried. The resulting mesoporous carbon was denoted as MC.

For co-impregnation of rhenium and ruthenium onto MC support, known amounts of ReCl<sub>5</sub> (Sigma–Aldrich) and RuCl<sub>3</sub>·xH<sub>2</sub>O (Sigma–Aldrich) as metal precursors were dissolved in 5 ml of acetone. During this process, Re:Ru molar ratio was adjusted to be 1:0, 0.75:0.25, 0.50:0.50, 0.25:0.75, and 0:1, while the total loading of

two metals was fixed at 0.6 mol% in all the samples to maintain the same number of active sites. The acetone solution containing metal precursors was then introduced to MC by an incipient wetness impregnation method. After drying the impregnated sample at 60 °C, it was calcined at 500 °C for 4 h with a heating rate of 5 °C/min under N<sub>2</sub> flow (50 ml/min) to remove chlorine and organic impurities. The prepared Re–Ru bimetallic catalysts were denoted as (0.6 – x)Re–xRu/MC (x = 0, 0.15, 0.3, 0.45, and 0.6), where x represented the ruthenium content (mol%).

### 2.2. Characterization

Textural properties of calcined (0.6 – x)Re–xRu/MC (x = 0, 0.15, 0.3, 0.45, and 0.6) catalysts were investigated by nitrogen adsorption–desorption measurements using a BELSORP-mini II instrument (BEL Japan). Surface areas of the catalysts were calculated by the Brunauer–Emmett–Teller (BET) method. The Re:Ru molar ratios of the catalysts were determined by ICP-MS analyses (ELAN 6100, Perkin–Elmer SCIEX). Temperature-programmed reduction (TPR) analyses of the calcined catalysts were conducted in a flow reactor system equipped with a quartz reactor. 10 mg of the catalysts was pretreated with N<sub>2</sub> flow (50 ml/min) at 200 °C for 1 h, and subsequently, TPR profiles were obtained using a thermal conductivity detector (TCD) at temperatures ranging from room temperature to 600 °C with a heating rate of 5 °C/min under 5% H<sub>2</sub>/N<sub>2</sub> flow (50 ml/min). X-ray diffraction (XRD) patterns of the reduced catalysts were collected by a D-Max2500-PC diffractometer (Rigaku) using Cu-K $\alpha$  radiation ( $\lambda = 1.541 \text{ \AA}$ ) operated at 50 kV and 100 mA. In order to investigate the metal surface area, metal dispersion, and average metal particle size of the reduced catalysts, CO chemisorption experiments were performed using a BELCAT-B instrument (BEL Japan). 10 mg of calcined catalyst was reduced at 500 °C for 4 h with a heating rate of 5 °C/min, and then 5% CO/He mixed gas was periodically injected at 100 °C. Metal surface area, metal dispersion, and average metal particle size were calculated from the amount of carbon monoxide adsorbed on the reduced catalyst by assuming that one carbon monoxide molecule occupies one surface metal atom. Morphology and particle size distribution of the reduced catalysts were examined by transmission electron microscopy (TEM) analyses (JEM-3010, JEOL). The particle size was calculated on the basis of projected area of particle in the TEM image by assuming that the shape of metal particle is sphere. The projected area, A, was converted to particle diameter, D, using  $D = 2(A/\pi)^{1/2}$ . To confirm the detailed distribution of rhenium and ruthenium of the reduced catalysts, energy dispersive X-ray spectroscopy (EDX) mapping analyses were conducted using a scanning transmission electron microscopy (STEM) apparatus (JEM-2100F, JEOL). Binding energies and surface atomic compositions of rhenium and ruthenium in the reduced catalysts were examined by X-ray photoelectron spectroscopy (XPS) analyses using a AXIS-HSI instrument (KRATOS) equipped with a Mg/Al anode source. For XPS analyses, the calcined catalysts were reduced using an ex situ reduction system at 500 °C for 4 h under 5% H<sub>2</sub>/N<sub>2</sub> flow (50 ml/min),

and the catalysts were then transported to glass jar with sample holder in argon atmosphere glove box to minimize air exposure. After outgassing the glass jar in a vacuum oven, the sample holder was transferred to the XPS chamber as quickly as possible. All the XPS spectra were calibrated using C 1s peak (284.5 eV) as a reference. H<sub>2</sub> temperature-programmed desorption (H<sub>2</sub>-TPD) analyses of the reduced catalysts were conducted using a BELCAT-B instrument (BEL Japan). 10 mg of calcined catalyst was reduced at 500 °C for 4 h with a heating rate of 5 °C/min under 5% H<sub>2</sub>/Ar flow (50 ml/min), and then purged with Ar flow (50 ml/min) for 10 min at 500 °C. After cooling the reduced catalyst to 200 °C under Ar flow (50 ml/min), 5% H<sub>2</sub>/Ar mixed gas (50 ml/min) was injected for 30 min at 200 °C. To remove physisorbed hydrogen, the sample was purged at 200 °C with Ar flow (50 ml/min), and subsequently, H<sub>2</sub>-TPD measurements were conducted within temperature range of 200–700 °C at a heating rate of 5 °C/min under Ar flow (50 ml/min).

### 2.3. Hydrogenation of succinic acid to BDO

Liquid-phase hydrogenation of succinic acid to BDO was conducted in a stainless steel autoclave reactor with a volume of 200 ml. Prior to the reaction, the catalysts were reduced using an ex situ reduction system at 500 °C for 4 h with a heating rate of 5 °C/min under 5% H<sub>2</sub>/N<sub>2</sub> flow (50 ml/min). In order to avoid air exposure, reduced catalyst (0.1 g), succinic acid (0.25 g), and 1,4-dioxane (50 ml, an inert aprotic solvent) were charged into the reactor in an argon atmosphere glove box. The closed reactor filled with argon was then mounted to the autoclave chamber as quickly as possible. After purging the reactor with nitrogen, it was pressurized up to 50 bar using hydrogen. The sealed autoclave was heated to the reaction temperature (200 °C), and then pressurized up to 80 bar using hydrogen. Catalytic reaction was conducted with constant stirring (700 rpm) for 7 h. After the reaction, the reactor was cooled to room temperature and depressurized. Reaction products were analyzed with a gas chromatograph (Younglin, ACME-6100) equipped with a flame ionization detector (FID). Conversion of succinic acid, selectivity for product, and yield for product were calculated according to the following equations.

$$\text{Conversion of succinic acid (\%)} = \frac{\text{mole of succinic acid reacted}}{\text{mole of succinic acid supplied}} \times 100 \quad (1)$$

$$\text{Selectivity for product (\%)} = \frac{\text{mole of product formed}}{\text{mole of succinic acid reacted}} \times 100 \quad (2)$$

$$\text{Yield for product (\%)} = \frac{\text{conversion of succinic acid} \times \text{selectivity for product}}{100} \quad (3)$$

Turnover frequency (TOF) and TOF for BDO (TOF<sub>BDO</sub>) were calculated on the basis of moles of succinic acid converted at ca. 10% conversion and moles of BDO formed at ca. 70% yield for GBL, respectively. The moles of surface metal atoms used for TOF and TOF<sub>BDO</sub> calculation were obtained by CO chemisorption experiments.

## 3. Results and discussion

### 3.1. Textural properties of (0.6-x)Re-xRu/MC catalysts

Textural properties of (0.6-x)Re-xRu/MC ( $x=0, 0.15, 0.3, 0.45$ , and  $0.6$ ) catalysts were examined by nitrogen adsorption-desorption measurements as shown in Fig. 2. All the catalysts exhibited IV-type isotherms indicative of mesoporous structure. H3-type hysteresis loops were also observed in the isotherms, which were attributed to the capillary condensation of nitrogen molecules in the well-developed mesopores of carbon support [23]. Detailed textural properties of (0.6-x)Re-xRu/MC ( $x=0, 0.15, 0.3, 0.45$ , and  $0.6$ ) catalysts are listed in Table 1. It was found that the actual Re:Ru loadings and molar ratios of the prepared catalysts were in good agreement with the designed

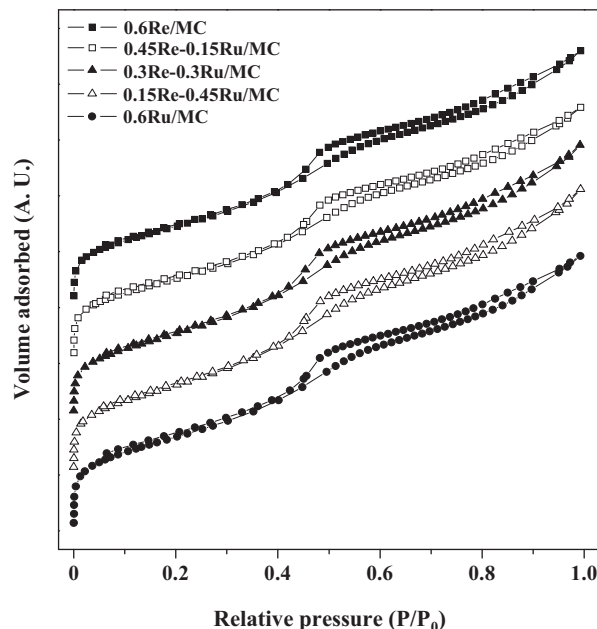


**Fig. 2.** Nitrogen adsorption–desorption isotherms of (0.6-x)Re-xRu/MC ( $x=0, 0.15, 0.3, 0.45$ , and  $0.6$ ) catalysts.

values. Total metal loadings were also well fixed at 0.6 mol%. All the catalysts retained high surface area ( $>812 \text{ m}^2/\text{g}$ ), large pore volume ( $>1.06 \text{ cm}^3/\text{g}$ ), and large average pore diameter ( $>5.0 \text{ nm}$ ), which means that mesoporous carbon structure were successfully formed by a single-step surfactant-templating method. Interestingly, surface area and pore volume of the catalysts decreased with increasing rhenium loading. This might be because pore blockage by rhenium was more severe than that by ruthenium due to the difference in atomic radius of rhenium (137 pm) and ruthenium (134 pm).

### 3.2. Reduction behaviors of (0.6-x)Re-xRu/MC catalysts

In order to investigate the reduction behaviors of (0.6-x)Re-xRu/MC ( $x=0, 0.15, 0.3, 0.45$ , and  $0.6$ ) catalysts, TPR measurements were conducted as shown in Fig. 3. It was found that 0.6Re/MC and 0.6Ru/MC catalysts exhibited asymmetrical reduction peaks at 340 °C and 264 °C, respectively; the former was attributed to the reduction of rhenium species [24], while the latter was attributed to the reduction of ruthenium species [25]. The reduction peak of 0.45Re-0.15Ru/MC catalyst moved toward lower temperature and showed more narrow shape than that of 0.6Re/MC. In case of bimetallic catalysts containing noble metals such as Pd, Pt, and Ru, the noble metals can affect the reduction of the other metal due to hydrogen transfer from their reduced species [26–29]. Therefore, it can be inferred that hydrogen adsorbed on reduced ruthenium species was transferred to unreduced neighboring rhenium species during the reduction process, which promoted the reduction of rhenium species. It is interesting to note that (0.6-x)Re-xRu/MC ( $x=0.15, 0.3$ , and  $0.45$ ) catalysts retained only one reduction peak corresponding to co-reduction of rhenium and ruthenium without any reduction peaks for bulk rhenium and ruthenium species, indicating that most of ruthenium atoms were distributed in the periphery of unreduced rhenium atoms throughout the catalyst. Furthermore, the reduction bands of (0.6-x)Re-xRu/MC ( $x=0.15, 0.3$ , and  $0.45$ ) catalysts were changed to the symmetrical shape compared to those of 0.6Re/MC and 0.6Ru/MC. It is known that the symmetrical peak shape can be induced from uniform reduction process caused

**Table 1**

Textural properties of  $(0.6 - x)\text{Re}-x\text{Ru}/\text{MC}$  ( $x = 0, 0.15, 0.3, 0.45$ , and  $0.6$ ) catalysts.

Sample	Re:Ru loading (mol%) <sup>a</sup>	Re:Ru molar ratio	Surface area ( $\text{m}^2/\text{g}$ ) <sup>b</sup>	Pore volume ( $\text{cm}^3/\text{g}$ ) <sup>c</sup>	Pore diameter (nm) <sup>d</sup>
0.6Re/MC	0.59:0	1:0	812	1.06	5.2
0.45Re-0.15Ru/MC	0.44:0.15	0.74:0.26	838	1.07	5.1
0.3Re-0.3Ru/MC	0.29:0.31	0.49:0.51	861	1.14	5.3
0.15Re-0.45Ru/MC	0.15:0.45	0.25:0.75	899	1.18	5.3
0.6Ru/MC	0:0.6	0:1	923	1.19	5.0

<sup>a</sup> Determined by ICP-MS measurement.

<sup>b</sup> Calculated by the BET equation.

<sup>c</sup> Total pore volume at  $P/P_0 = 0.99$ .

<sup>d</sup> Average pore diameter.

**Table 2**

TPR and CO chemisorption results of  $(0.6 - x)\text{Re}-x\text{Ru}/\text{MC}$  ( $x = 0, 0.15, 0.3, 0.45$ , and  $0.6$ ) catalysts.

Catalyst	Amount of hydrogen uptake (mol-H <sub>2</sub> /mol-metal) <sup>a</sup>	Metal surface area ( $\text{m}^2/\text{g}$ -catalyst) <sup>b</sup>	Metal dispersion (%) <sup>b</sup>	Average metal particle size (nm) <sup>b</sup>
0.6Re/MC	2.73	3.15	17.6	7.9
0.45Re-0.15Ru/MC	3.29	3.62	20.3	6.8
0.3Re-0.3Ru/MC	4.10	4.74	26.9	5.1
0.15Re-0.45Ru/MC	3.50	4.09	23.2	5.9
0.6Ru/MC	3.03	3.36	19.2	6.9

<sup>a</sup> Calculated from peak area of TPR profiles in Fig. 3.

<sup>b</sup> Calculated from CO chemisorption measurement by assuming a stoichiometry factor of  $\text{CO}/\text{metal atom} = 1$ .

by homogeneity of metal particle size [30]. Thus, it is inferred that the particles of both rhenium and ruthenium species were homogeneously formed in the Re-Ru bimetallic catalysts. The amounts of hydrogen uptake calculated from the TPR profiles of  $(0.6 - x)\text{Re}-x\text{Ru}/\text{MC}$  ( $x = 0, 0.15, 0.3, 0.45$ , and  $0.6$ ) catalysts are summarized in Table 2. It was found that  $(0.6 - x)\text{Re}-x\text{Ru}/\text{MC}$  ( $x = 0.15, 0.3$ , and  $0.45$ ) catalysts showed the larger amount of hydrogen uptake than  $0.6\text{Re}/\text{MC}$  and  $0.6\text{Ru}/\text{MC}$ , indicating that the interaction between rhenium and ruthenium species might modify the reducibility of both metal species. However, the amount of hydrogen uptake of  $(0.6 - x)\text{Re}-x\text{Ru}/\text{MC}$  ( $x = 0.15, 0.3, 0.45$ , and  $0.6$ ) catalysts determined by TPR measurements exceeded the theoretical ratio of hydrogen with respect to rhenium (3.5) and ruthenium (2) for complete reduction [31]. This was due to hydrogen spillover induced by metal surface on carbon material

[32]. Therefore, it is difficult to determine the reduction degree of  $(0.6 - x)\text{Re}-x\text{Ru}/\text{MC}$  ( $x = 0.15, 0.3, 0.45$ , and  $0.6$ ) catalysts by only TPR results, and this issue will be further discussed in Section 3.5.

### 3.3. Crystalline structures of reduced $(0.6 - x)\text{Re}-x\text{Ru}/\text{MC}$ catalysts

Crystalline phases of the reduced  $(0.6 - x)\text{Re}-x\text{Ru}/\text{MC}$  ( $x = 0, 0.15, 0.3, 0.45$ , and  $0.6$ ) catalysts were examined by XRD measurements as presented in Fig. 4. All the catalysts showed diffraction peaks for graphitic carbon structure at  $2\theta = 23.5^\circ$  and  $43.8^\circ$  [33]. The diffraction peaks corresponding to  $(101)$  planes of metallic rhenium (dashed line in Fig. 4) and ruthenium (solid line in Fig. 4) were

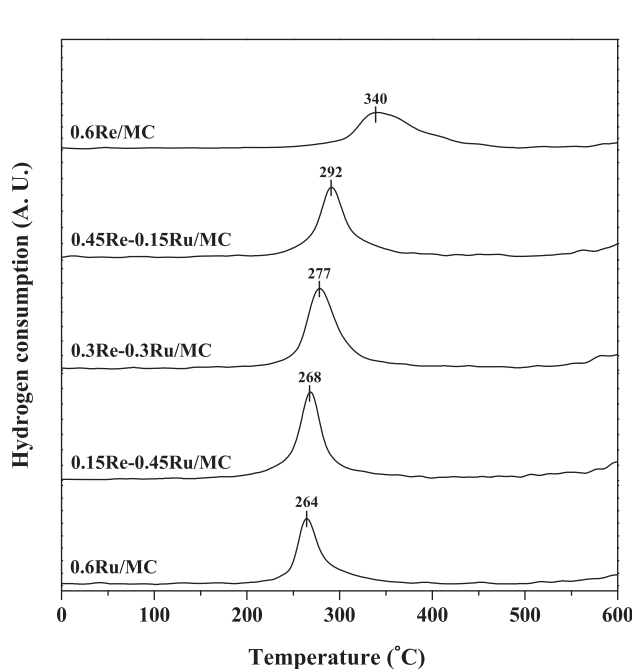


Fig. 3. TPR profiles of  $(0.6 - x)\text{Re}-x\text{Ru}/\text{MC}$  ( $x = 0, 0.15, 0.3, 0.45$ , and  $0.6$ ) catalysts.

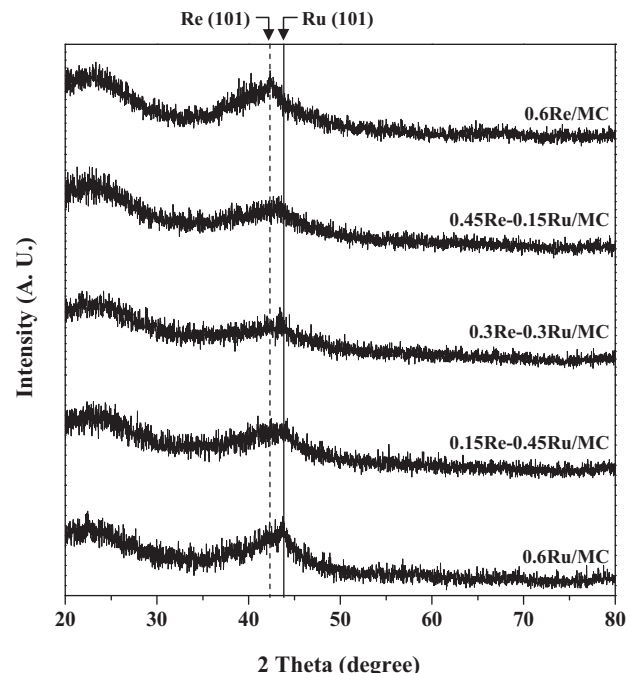
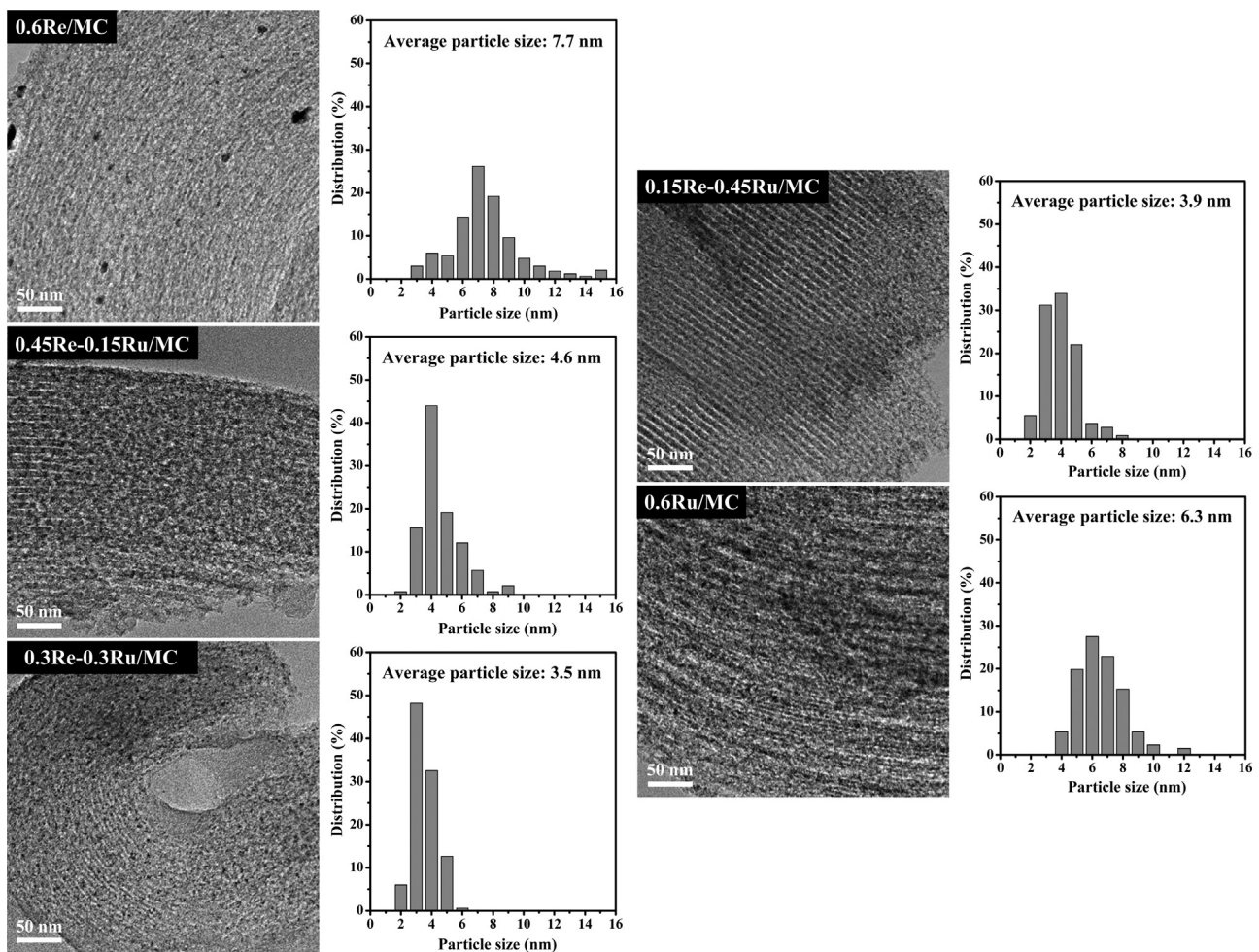


Fig. 4. XRD patterns of reduced  $(0.6 - x)\text{Re}-x\text{Ru}/\text{MC}$  ( $x = 0, 0.15, 0.3, 0.45$ , and  $0.6$ ) catalysts.



**Fig. 5.** TEM images and particle size distributions of reduced  $(0.6 - x)\text{Re}-x\text{Ru}/\text{MC}$  ( $x = 0, 0.15, 0.3, 0.45$ , and  $0.6$ ) catalysts.

clearly observed in the XRD patterns of  $0.6\text{Re}/\text{MC}$  and  $0.6\text{Ru}/\text{MC}$  catalysts, respectively, although the diffraction peak of  $0.6\text{Ru}/\text{MC}$  was overlapped with that ( $43.8^\circ$ ) of the carbon support. On the other hand, any diffraction peaks for rhenium and ruthenium species were not detected in the  $(0.6 - x)\text{Re}-x\text{Ru}/\text{MC}$  ( $x = 0.15, 0.3$ , and  $0.45$ ) catalysts. This result might be because particle sizes of metallic rhenium and ruthenium in the catalysts were too small to be detected by XRD. According to the literatures [18–20], rhenium and ruthenium species can interact in all range of chemical composition due to their similar crystal structure, atomic radius, and electronegativity. Thus, it is inferred that the interaction between rhenium and ruthenium species affected the development of particles during the reduction process, which might induce the decrement of metal particle size of Re–Ru bimetallic catalysts compared to rhenium or ruthenium monometallic catalyst.

#### 3.4. Metal dispersion of reduced $(0.6 - x)\text{Re}-x\text{Ru}/\text{MC}$ catalysts

To investigate the effect of Re–Ru interaction on the metal dispersion, CO chemisorption measurements for the reduced  $(0.6 - x)\text{Re}-x\text{Ru}/\text{MC}$  ( $x = 0, 0.15, 0.3, 0.45$ , and  $0.6$ ) catalysts were conducted. As listed in Table 2, metal surface area and metal dispersion increased in the order of  $0.6\text{Re}/\text{MC} < 0.6\text{Ru}/\text{MC} < 0.45\text{Re}-0.15\text{Ru}/\text{MC} < 0.15\text{Re}-0.45\text{Ru}/\text{MC} < 0.3\text{Re}-0.3\text{Ru}/\text{MC}$ , while average metal particle size decreased in the order of  $0.6\text{Re}/\text{MC} > 0.6\text{Ru}/\text{MC} > 0.45\text{Re}-0.15\text{Ru}/\text{MC} > 0.15\text{Re}-0.45\text{Ru}/\text{MC} > 0.3\text{Re}-0.3\text{Ru}/\text{MC}$ . It was found that all the catalysts retained small metal particle size in the range of  $5.1$ – $7.9$  nm, indicating that metallic rhenium

and ruthenium particles were finely dispersed in the mesoporous carbon framework. It is noteworthy that average metal particle sizes of  $(0.6 - x)\text{Re}-x\text{Ru}/\text{MC}$  ( $x = 0.15, 0.3$ , and  $0.45$ ) catalysts were smaller than those of  $0.6\text{Re}/\text{MC}$  and  $0.6\text{Ru}/\text{MC}$ . This might be because aggregation of each rhenium and ruthenium particle was effectively suppressed by forming a Re–Ru metallic bond during the reduction process, as discussed in the XRD results.

The above result was further confirmed by TEM analyses. Fig. 5 shows the TEM images and particle size distributions of reduced  $(0.6 - x)\text{Re}-x\text{Ru}/\text{MC}$  ( $x = 0, 0.15, 0.3, 0.45$ , and  $0.6$ ) catalysts. All the catalysts retained an ordered mesoporous carbon structure and well-dispersed metal particles as presented in the TEM images. However,  $(0.6 - x)\text{Re}-x\text{Ru}/\text{MC}$  ( $x = 0.15, 0.3$ , and  $0.45$ ) catalysts showed more narrow particle size distributions than  $0.6\text{Re}/\text{MC}$  and  $0.6\text{Ru}/\text{MC}$ , indicating that metal particles of Re–Ru bimetallic catalysts were uniformly distributed, as discussed in the TPR results. It is noteworthy that all the reduced catalysts retained a few metal particles which were larger than pore sizes of the calcined catalysts (Table 1). This means that some metal particles grown during the reduction process caused the partial pore blockage of carbon supports. It was revealed that average metal particle size measured by TEM decreased in the order of  $0.6\text{Re}/\text{MC} > 0.6\text{Ru}/\text{MC} > 0.45\text{Re}-0.15\text{Ru}/\text{MC} > 0.15\text{Re}-0.45\text{Ru}/\text{MC} > 0.3\text{Re}-0.3\text{Ru}/\text{MC}$ , which was well consistent with the trend of average metal particle size determined by CO chemisorption. However, average metal particle sizes of all catalysts determined by CO chemisorption were larger than those measured by TEM. This overestimation might be because the catalysts were partially

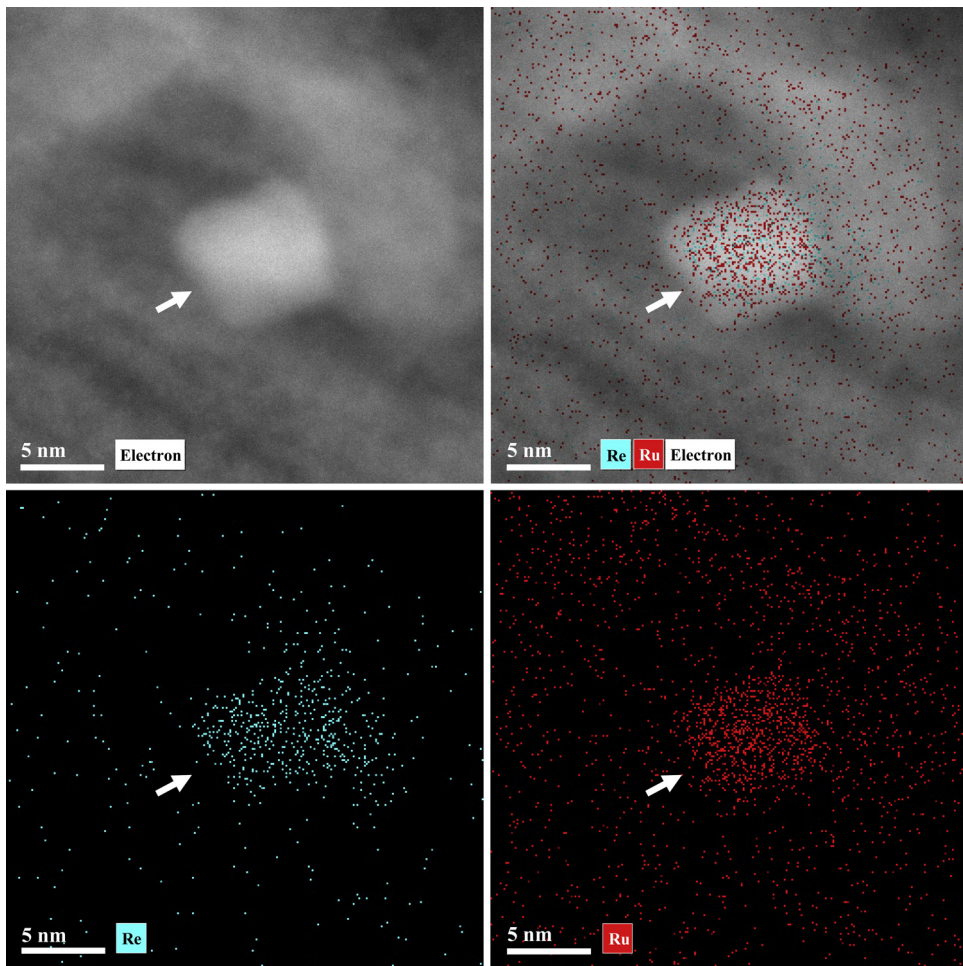


**Fig. 6.** STEM-EDX images of reduced 0.3Re–0.3Ru/MC catalyst obtained by mapping on rhenium and ruthenium. (For interpretation of the references to color in text near the figure citation, the reader is referred to the web version of this article.)

reduced under the reduction condition at 500 °C for 4 h. Among the catalysts, 0.3Re–0.3Ru/MC showed the largest metal dispersion and smallest average metal particle size.

In order to confirm the distribution of rhenium and ruthenium species, STEM-EDX analyses were carried out. Fig. 6 showed the STEM and EDX mapping images for one metal particle (white arrow in Fig. 6) of reduced 0.3Re–0.3Ru/MC catalyst. Rhenium and ruthenium species were distinguishable in the EDX mapping images. It is noticeable that rhenium atom (blue dot in Fig. 6) and ruthenium atom (red dot in Fig. 6) were co-presented in the metal particle domain of 0.3Re–0.3Ru/MC catalyst. On the basis of TPR, XRD, and EDX mapping results, it is believed that a Re–Ru miscible phase was formed in the reduced 0.3Re–0.3Ru/MC catalyst and this was responsible for strong interaction between metallic rhenium and ruthenium species.

### 3.5. XPS study of reduced $(0.6 - x)\text{Re}-x\text{Ru}/\text{MC}$ catalysts

It is known that the oxidation state of metal species in the catalyst served as an important factor determining the catalytic activity [34,35]. Accordingly, the oxidation states of reduced  $(0.6 - x)\text{Re}-x\text{Ru}/\text{MC}$  ( $x = 0, 0.15, 0.3, 0.45$ , and  $0.6$ ) catalysts were examined by XPS analyses. Fig. 7 shows the XPS spectra for Re 4f (Fig. 7(a)) and Ru 3p<sub>3/2</sub> (Fig. 7(b)) levels of the catalysts. The Re 4f spectra were deconvoluted into Re 4f<sub>7/2</sub> (solid line in Fig. 7(a)) and Re 4f<sub>5/2</sub> (dashed line in Fig. 7(a)) peaks, and then Re 4f<sub>7/2</sub> spectra

were divided into  $\text{Re}^0$  (40.6 eV),  $\text{Re}^{3+}$  (41.4 eV),  $\text{Re}^{4+}$  (42.3 eV), and  $\text{Re}^{6+}$  (45.3 eV) species [36,37]. On the other hand, the Ru 3p<sub>3/2</sub> spectra were assigned to metallic  $\text{Ru}^0$  (462.1 eV) and  $\text{Ru}^{4+}$  (464.3 eV) species [38]. It was found that the areas of Re 4f and Ru 3p<sub>3/2</sub> spectra decreased with decreasing the rhenium and ruthenium loading, respectively. On the basis of deconvoluted peak areas of Re 3f<sub>7/2</sub> and Ru 3p<sub>3/2</sub> spectra, the oxidation state ratios and surface atomic ratios of rhenium and ruthenium were quantified as summarized in Table 3. It was found that  $\text{Re}^0/\text{Re}_{\text{total}}$  increased in the order of  $0.6\text{Re}/\text{MC} < 0.15\text{Re}-0.45\text{Ru}/\text{MC} < 0.45\text{Re}-0.15\text{Ru}/\text{MC} < 0.3\text{Re}-0.3\text{Ru}/\text{MC}$ , while  $\text{Ru}^0/\text{Ru}_{\text{total}}$  increased in the order of  $0.6\text{Ru}/\text{MC} < 0.15\text{Re}-0.45\text{Ru}/\text{MC} < 0.45\text{Re}-0.15\text{Ru}/\text{MC} < 0.3\text{Re}-0.3\text{Ru}/\text{MC}$ . It was also found that  $(\text{Re}^0 + \text{Ru}^0)/\text{C}$  increased in the order of  $0.6\text{Re}/\text{MC} < 0.6\text{Ru}/\text{MC} < 0.45\text{Re}-0.15\text{Ru}/\text{MC} < 0.15\text{Re}-0.45\text{Ru}/\text{MC} < 0.3\text{Re}-0.3\text{Ru}/\text{MC}$ , which was in good agreement with the trend of metal surface area determined by CO chemisorption (Table 2). This demonstrates that all the catalysts retained different total reduction degree of rhenium and ruthenium species. In addition,  $(\text{Re}^0 + \text{Ru}^0)/\text{C}$  increased with decreasing average metal particle size determined by TEM (Fig. 5), indicating that total reduction degree of both two metals was closely related to the average particle size of the catalysts. It is important to note that  $(\text{Re}^0 + \text{Ru}^0)/\text{C}$  ratios of  $(0.6 - x)\text{Re}-x\text{Ru}/\text{MC}$  ( $x = 0.15, 0.3$ , and  $0.45$ ) catalysts were higher than those of  $0.6\text{Re}/\text{MC}$  and  $0.6\text{Ru}/\text{MC}$ . According to the shrinking core model [39–41], the reduction of a metal particle is limited by the intraparticle hydrogen diffusivity,

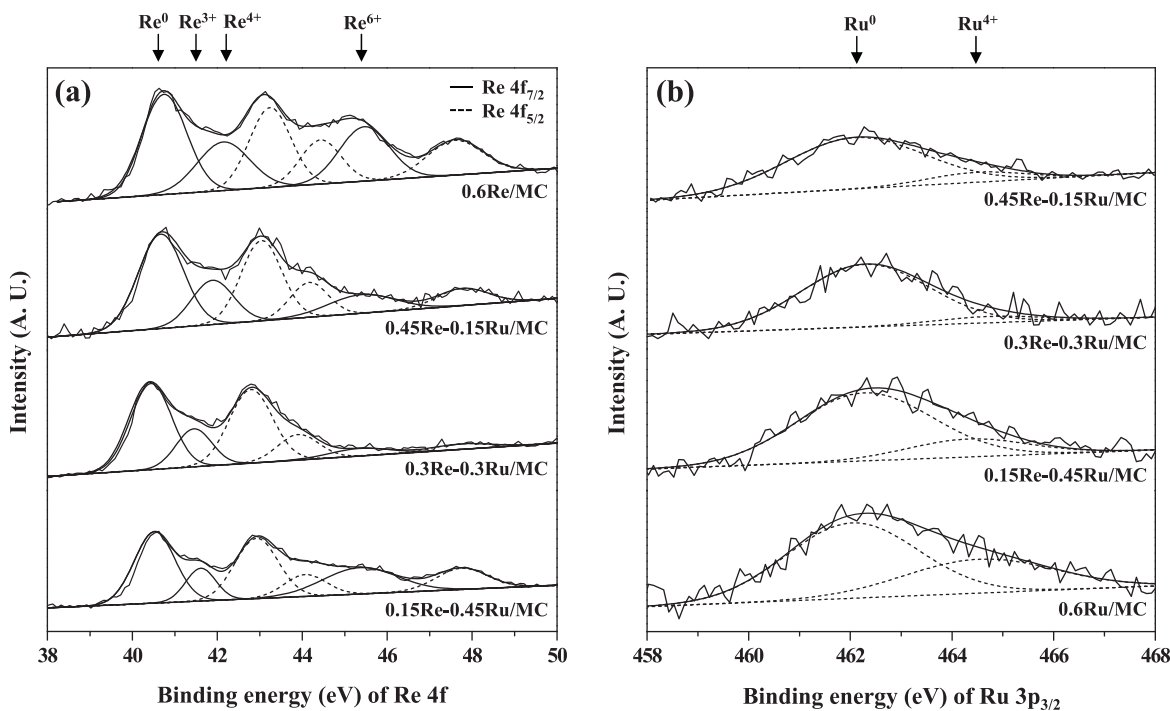


**Fig. 7.** XPS spectra of (a) Re 4f and (b) Ru 3p<sub>3/2</sub> levels in the reduced (0.6 – x)Re–xRu/MC ( $x = 0, 0.15, 0.3, 0.45$ , and 0.6) catalysts.

which means that the reduction degree of metal species can be enhanced by decreasing the particle size. Therefore, it is believed that the Re–Ru bimetallic catalysts with smaller particle size were more effectively reduced than rhenium or ruthenium monometallic catalyst.

### 3.6. Hydrogen adsorption study on reduced (0.6 – x)Re–xRu/MC catalysts

It has been reported that the ability of hydrogen adsorption on the active sites plays a crucial role in the catalytic hydrogenation reaction [42,43]. Thus, H<sub>2</sub>-TPD measurements were carried out to explain the affinity of metal species toward hydrogen in the reduced (0.6 – x)Re–xRu/MC ( $x = 0, 0.15, 0.3, 0.45$ , and 0.6) catalysts. In this study, hydrogen was injected to the reduced catalysts at 200 °C, which was identical to the reaction temperature, to thermally activate the dissociative adsorption of hydrogen molecules on metallic rhenium and ruthenium [21,22,44]. Fig. 8 shows the H<sub>2</sub>-TPD profiles of reduced (0.6 – x)Re–xRu/MC ( $x = 0, 0.15, 0.3, 0.45$ , and 0.6) catalysts. For comparison, H<sub>2</sub>-TPD profile of MC support was also presented. The H<sub>2</sub>-TPD profile of MC support exhibited a broad minor peak at 283 °C and a main peak at 607 °C; the former corresponded to the adsorption of hydrogen molecules, while the latter was caused by gaseous products such as H<sub>2</sub>, CH<sub>4</sub>, C<sub>2</sub>H<sub>2</sub>, and C<sub>2</sub>H<sub>4</sub> formed by reaction of carbon with

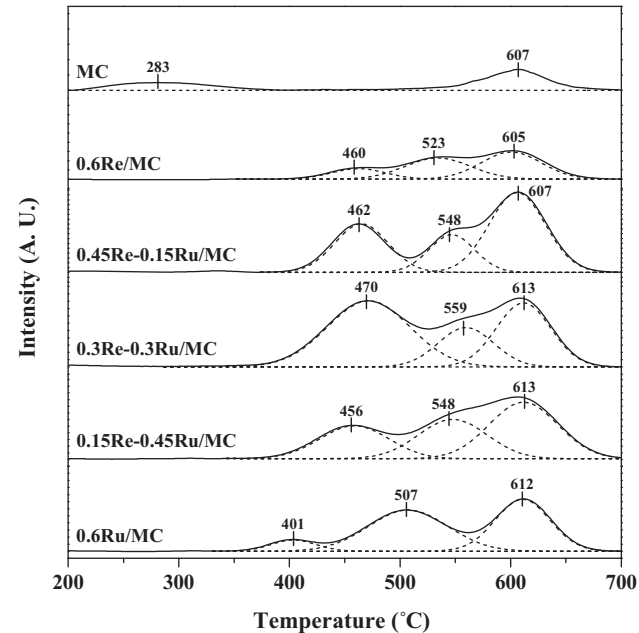


**Fig. 8.** H<sub>2</sub>-TPD profiles of reduced (0.6 – x)Re–xRu/MC ( $x = 0, 0.15, 0.3, 0.45$ , and 0.6) catalysts and mesoporous carbon (MC) support.

**Table 3**

XPS analyses results of reduced (0.6 – x)Re–xRu/MC ( $x = 0, 0.15, 0.3, 0.45$ , and 0.6) catalysts.

Catalyst	Ratio of rhenium species <sup>a</sup>			Ratio of ruthenium species <sup>a</sup>		Surface atomic ratio ( $\times 10^3$ )		
	$\text{Re}^0/\text{Re}_{\text{total}}$	$\text{Re}^{\alpha+}/\text{Re}_{\text{total}}$ <sup>b</sup>	$\text{Re}^{6+}/\text{Re}_{\text{total}}$	$\text{Ru}^0/\text{Ru}_{\text{total}}$	$\text{Ru}^{4+}/\text{Ru}_{\text{total}}$	$\text{Re}_{\text{total}}/\text{C}$	$\text{Ru}_{\text{total}}/\text{C}$	$(\text{Re}^0 + \text{Ru}^0)/\text{C}$
0.6Re/MC	0.46	0.26	0.28	–	–	4.12	–	1.90
0.45Re-0.15Ru/MC	0.61	0.24	0.15	0.88	0.12	5.03	1.81	4.66
0.3Re-0.3Ru/MC	0.67	0.25	0.08	0.92	0.08	4.75	5.46	8.21
0.15Re-0.45Ru/MC	0.53	0.16	0.31	0.81	0.19	1.51	6.65	6.19
0.6Ru/MC	–	–	–	0.65	0.35	–	5.73	3.72

<sup>a</sup> Calculated from deconvoluted peak area of XPS spectra in Fig. 7.

<sup>b</sup>  $3 \leq \alpha \leq 4$ .

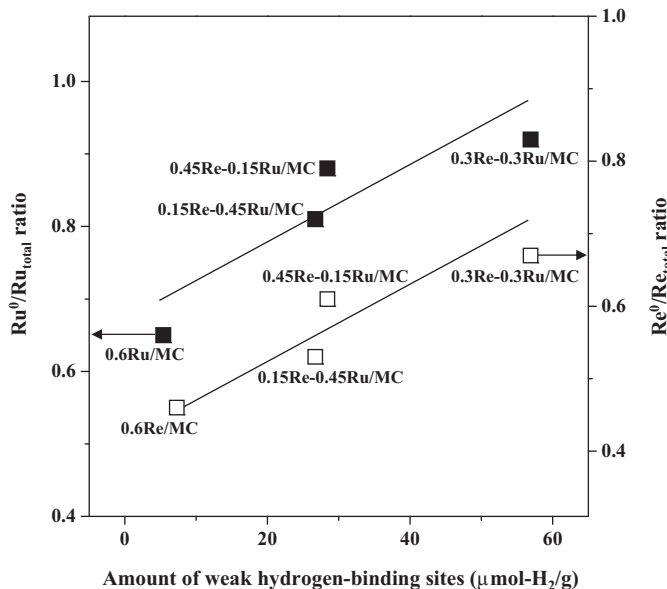


**Fig. 9.** Correlations between the amount of weak hydrogen-binding sites and  $\text{Re}^0/\text{Re}_{\text{total}}$  ratio and between the amount of weak hydrogen-binding sites and  $\text{Ru}^0/\text{Ru}_{\text{total}}$  ratio of reduced  $(0.6 - x)\text{Re}-x\text{Ru}/\text{MC}$  ( $x = 0, 0.15, 0.3, 0.45$ , and  $0.6$ ) catalysts.

spillover hydrogen on carbon surface, as evidenced by the TPR results [32,33,45]. Interestingly, when rhenium or ruthenium was added into the MC support, new peaks corresponding to the dissociatively adsorbed hydrogen ( $400\text{--}600^\circ\text{C}$ ) appeared instead of the peak for molecularly adsorbed hydrogen ( $<300^\circ\text{C}$ ). In order to distinguish dissociatively adsorbed hydrogen in the  $\text{H}_2\text{-TPD}$  profiles of the reduced  $(0.6 - x)\text{Re}-x\text{Ru}/\text{MC}$  catalysts, therefore,  $\text{H}_2\text{-TPD}$  profiles were deconvoluted into three peaks in terms of desorption temperature; weak hydrogen-binding site ( $400\text{--}500^\circ\text{C}$ ), strong hydrogen-binding site ( $500\text{--}600^\circ\text{C}$ ), and the others ( $>600^\circ\text{C}$ ). The other peaks appearing above  $600^\circ\text{C}$  might be due to mesoporous carbon. Thus, weak hydrogen-binding sites and strong hydrogen-binding sites were only considered for quantification. The amounts of these two hydrogen-binding sites calculated from the deconvoluted results of  $\text{H}_2\text{-TPD}$  profiles of the catalysts are summarized in Table 4. Total amount of hydrogen desorbed from the reduced  $(0.6 - x)\text{Re}-x\text{Ru}/\text{MC}$  catalysts increased in the order of  $0.6\text{Re}/\text{MC} < 0.6\text{Ru}/\text{MC} < 0.45\text{Re}-0.15\text{Ru}/\text{MC} < 0.15\text{Re}-0.45\text{Ru}/\text{MC} < 0.3\text{Re}-0.3\text{Ru}/\text{MC}$ . This trend was well consistent with the trend of  $(\text{Re}^0 + \text{Ru}^0)/\text{C}$  determined by XPS analyses (Table 3), indicating that larger total amount of desorbed hydrogen resulted from more reduced state of the catalysts. On the other hand, the amount of weak hydrogen-binding sites increased in the order of  $0.6\text{Ru}/\text{MC} < 0.6\text{Re}/\text{MC} < 0.15\text{Re}-0.45\text{Ru}/\text{MC} < 0.45\text{Re}$

**Table 4**  
 $\text{H}_2\text{-TPD}$  results of reduced  $(0.6 - x)\text{Re}-x\text{Ru}/\text{MC}$  ( $x = 0, 0.15, 0.3, 0.45$ , and  $0.6$ ) catalysts.

Catalyst	Amount of desorbed hydrogen ( $\mu\text{mol-H}_2/\text{g-catalyst}$ ) <sup>a</sup>		Total
	Weak site ( $400\text{--}500^\circ\text{C}$ )	Strong site ( $500\text{--}600^\circ\text{C}$ )	
0.6Re/MC	7.3	15.5	22.8
0.45Re-0.15Ru/MC	28.4	18.9	47.3
0.3Re-0.3Ru/MC	56.9	23.2	80.1
0.15Re-0.45Ru/MC	26.7	28.4	52.1
0.6Ru/MC	5.4	35.6	41.0

<sup>a</sup> Calculated from deconvoluted peak area of  $\text{H}_2\text{-TPD}$  profiles in Fig. 8.

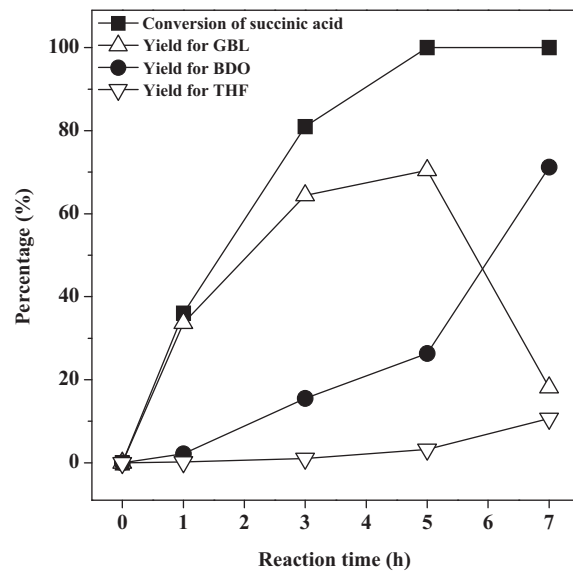


**Fig. 10.** Conversion of succinic acid and yields for GBL, BDO, and THF with time on stream in liquid-phase hydrogenation of succinic acid over  $0.3\text{Re}-0.3\text{Ru}/\text{MC}$  catalyst at  $200^\circ\text{C}$  and  $80$  bar.

$-0.15\text{Ru}/\text{MC} < 0.3\text{Re}-0.3\text{Ru}/\text{MC}$ , which was different from the trend of the total amount of hydrogen-binding sites.

From XPS and  $\text{H}_2\text{-TPD}$  results of the reduced  $(0.6 - x)\text{Re}-x\text{Ru}/\text{MC}$  catalysts, it was found that the trend of weak hydrogen-binding sites was well matched with the trend of  $\text{Re}^0/\text{Re}_{\text{total}}$  and  $\text{Ru}^0/\text{Ru}_{\text{total}}$  ratios (Table 3). Fig. 9 shows the relationships between the amount of weak hydrogen-binding sites and  $\text{Re}^0/\text{Re}_{\text{total}}$  ratio and between the amount of weak hydrogen-binding sites and  $\text{Ru}^0/\text{Ru}_{\text{total}}$  ratio of reduced  $(0.6 - x)\text{Re}-x\text{Ru}/\text{MC}$  ( $x = 0, 0.15, 0.3, 0.45$ , and  $0.6$ ) catalysts. It was revealed that the amount of weak hydrogen-binding sites increased with increasing  $\text{Re}^0/\text{Re}_{\text{total}}$  and  $\text{Ru}^0/\text{Ru}_{\text{total}}$  ratios, suggesting that the metallic ratio was a crucial factor determining the hydrogen adsorption behavior of  $(0.6 - x)\text{Re}-x\text{Ru}/\text{MC}$  catalysts. In other words, the synergistic interaction formed by Re–Ru metallic bond increased the amount of weak hydrogen-binding sites with respect to total active sites in the  $(0.6 - x)\text{Re}-x\text{Ru}/\text{MC}$  catalysts. It is well known that the weakly bound hydrogen atoms on the metallic surface are highly mobile due to their low stability, and therefore, they can be easily and continuously delivered to the adsorbed reactant molecules [46,47]. Thus, it is expected that a catalyst retaining larger amount of weak hydrogen-binding sites would be more favorable for continuous supply of hydrogen to adsorbed succinic acid.

### 3.7. Hydrogenation of succinic acid to BDO over $(0.6 - x)\text{Re}-x\text{Ru}/\text{MC}$ catalysts

In order to ensure the reaction pathways presented in Fig. 1, catalytic hydrogenation of succinic acid to BDO was carried out at  $200^\circ\text{C}$  and  $80$  bar with time on stream.  $0.3\text{Re}-0.3\text{Ru}/\text{MC}$  catalyst with the largest amount of weak hydrogen-binding sites was used as a model catalyst for the reaction. Fig. 10 shows the conversion of succinic acid and yields for GBL, BDO, and THF as a function of time. It was found that succinic acid was completely converted after  $5$  h, and yield for GBL exhibited a volcano-shaped curve with respect to the reaction time because GBL was transformed to BDO or THF by consecutive hydrogenation. It is noteworthy that BDO was dominantly produced from GBL, indicating that BDO can be selectively formed from succinic acid over  $0.3\text{Re}-0.3\text{Ru}/\text{MC}$  catalyst. The yield for BDO showed the maximum value (71.2%) after  $7$  h-reaction.

**Table 5**

Performance of  $(0.6-x)\text{Re}-x\text{Ru}/\text{MC}$  ( $x=0, 0.15, 0.3, 0.45$ , and  $0.6$ ) catalysts in liquid-phase hydrogenation of succinic acid at  $200^\circ\text{C}$  and  $80$  bar for  $7$  h.

Catalyst	Conversion of succinic acid (%)	Selectivity (%)			Yield for BDO (%)	TOF ( $\text{h}^{-1}$ ) <sup>a</sup>	$\text{TOF}_{\text{BDO}} (\text{h}^{-1})^{\text{b}}$
		GBL	BDO	THF			
0.6Re/MC	73.1	88.7	7.7	3.6	5.6	25.4	2.05
0.45Re-0.15Ru/MC	100	39.8	52.2	7.9	52.2	46.1	6.04
0.3Re-0.3Ru/MC	100	18.1	71.2	10.7	71.2	61.2	8.51
0.15Re-0.45Ru/MC	100	44.3	48.9	6.8	48.9	38.6	5.23
0.6Ru/MC	45.2	97.5	1.8	0.7	0.8	13.4	0.29

<sup>a</sup> Calculated as moles of succinic acid converted per moles of surface metal atom per hour (at ca. 10% conversion of succinic acid).

<sup>b</sup> Calculated as moles of BDO produced per moles of surface metal atom per hour (at ca. 70% yield for GBL).

The catalytic performance of  $(0.6-x)\text{Re}-x\text{Ru}/\text{MC}$  ( $x=0, 0.15, 0.3, 0.45$ , and  $0.6$ ) in the liquid-phase hydrogenation of succinic acid to BDO at  $200^\circ\text{C}$  and  $80$  bar for  $7$  h is summarized in Table 5. It was found that  $0.6\text{Re}/\text{MC}$  and  $0.6\text{Ru}/\text{MC}$  catalysts produced GBL as a major product, while  $(0.6-x)\text{Re}-x\text{Ru}/\text{MC}$  ( $x=0.15, 0.3$ , and  $0.45$ ) catalysts produced BDO as a major product in the reaction. This result indicates that Re–Ru bimetallic catalysts were more effective for consecutive hydrogenation of succinic acid to BDO via GBL than rhenium or ruthenium monometallic catalyst. It should be noted that TOF and  $\text{TOF}_{\text{BDO}}$  of  $(0.6-x)\text{Re}-x\text{Ru}/\text{MC}$  ( $x=0.15, 0.3$ , and  $0.45$ ) catalysts were also higher than those of  $0.6\text{Re}/\text{MC}$  and  $0.6\text{Ru}/\text{MC}$ , which means that the Re–Ru bimetallic catalysts were structure sensitive in the hydrogenation of succinic acid to BDO. In other words, the catalytic activity of  $(0.6-x)\text{Re}-x\text{Ru}/\text{MC}$  was significantly affected by the ability of active sites rather than by the amount of total active sites. TOF and  $\text{TOF}_{\text{BDO}}$  increased in the order of  $0.6\text{Ru}/\text{MC} < 0.6\text{Re}/\text{MC} < 0.15\text{Re}-0.45\text{Ru}/\text{MC} < 0.45\text{Re}-0.15\text{Ru}/\text{MC} < 0.3\text{Re}-0.3\text{Ru}/\text{MC}$ . Among the catalysts tested,  $0.3\text{Re}-0.3\text{Ru}/\text{MC}$  showed the highest TOF ( $61.2 \text{ h}^{-1}$ ) and  $\text{TOF}_{\text{BDO}}$  ( $8.51 \text{ h}^{-1}$ ). In particular, the catalytic performance of  $0.3\text{Re}-0.3\text{Ru}/\text{MC}$  was comparable to that of reported Re-based bimetallic catalysts [14–17]. This implies that  $0.3\text{Re}-0.3\text{Ru}/\text{MC}$  served as a promising catalyst for the selective formation of BDO from succinic acid.

From the trend of  $\text{TOF}_{\text{BDO}}$  (Table 5), it was revealed that an optimal Re:Ru molar ratio was required for the maximum BDO production by hydrogenation of succinic acid over  $(0.6-x)\text{Re}-x\text{Ru}/\text{MC}$  ( $x=0, 0.15, 0.3, 0.45$ , and  $0.6$ ) catalysts. It was also found

that the trend of  $\text{TOF}_{\text{BDO}}$  was closely related to the hydrogen adsorption behavior of the catalysts. Accordingly,  $\text{TOF}_{\text{BDO}}$  of  $(0.6-x)\text{Re}-x\text{Ru}/\text{MC}$  catalysts was correlated with the amount of weak hydrogen-binding sites as shown in Fig. 11. It was revealed that  $\text{TOF}_{\text{BDO}}$  increased with increasing the amount of weak hydrogen-binding sites. This indicates that weak hydrogen-binding sites of the catalysts served as the crucial active sites for the selective formation of BDO from hydrogenation of succinic acid. This is because weak hydrogen-binding site can provide excellent hydrogen supply to the reactants adsorbed on the catalysts, as discussed in the H<sub>2</sub>-TPD results. Among the catalysts,  $0.3\text{Re}-0.3\text{Ru}/\text{MC}$  catalyst with the largest amount of weak hydrogen-binding sites showed the highest  $\text{TOF}_{\text{BDO}}$  in the hydrogenation of succinic acid to BDO.

### 3.8. Stability and reusability of $0.3\text{Re}-0.3\text{Ru}/\text{MC}$ catalysts

To investigate the stability of  $0.3\text{Re}-0.3\text{Ru}/\text{MC}$  catalyst, reusability of the catalyst was tested. According to the previous works [12,13], it was revealed that the decrement of catalytic activity in the hydrogenation of succinic acid was mainly attributed to the leaching of active metal species under the harsh reaction conditions. For the recycle test, the spent catalyst was separated from liquid product by filtration, washed with deionized water, and dried in a vacuum oven at  $60^\circ\text{C}$  after each reaction test. The remaining liquid containing leached metal species was collected for ICP-MS analysis. Fig. 12 shows the recycle results of  $0.3\text{Re}-0.3\text{Ru}/\text{MC}$  catalyst in the liquid-phase hydrogenation of succinic acid to BDO at

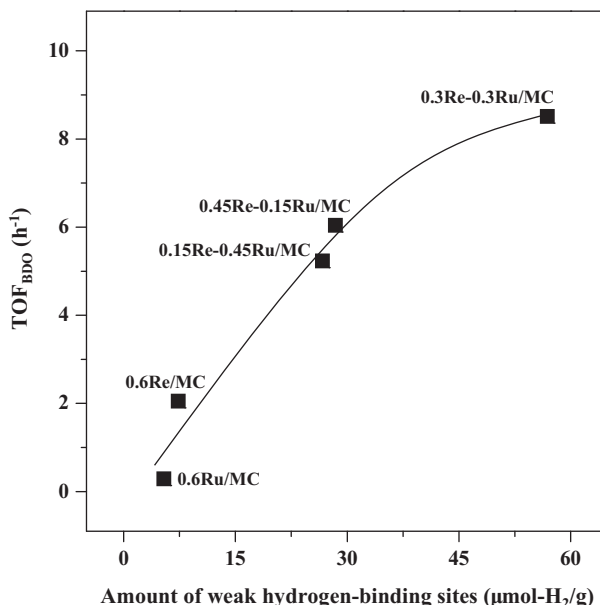


Fig. 11. A correlation between  $\text{TOF}_{\text{BDO}}$  and the amount of weak hydrogen-binding sites in the reduced  $(0.6-x)\text{Re}-x\text{Ru}/\text{MC}$  ( $x=0, 0.15, 0.3, 0.45$ , and  $0.6$ ) catalysts.

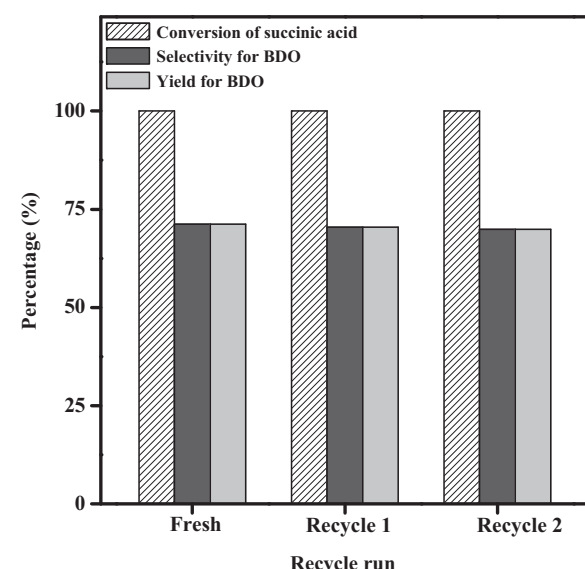


Fig. 12. Results for liquid-phase hydrogenation of succinic acid to BDO over  $0.3\text{Re}-0.3\text{Ru}/\text{MC}$  catalyst with respect to recycle run at  $200^\circ\text{C}$  and  $80$  bar for  $7$  h.

**Table 6**

Metal leaching in the liquid-phase hydrogenation of succinic acid over 0.3Re–0.3Ru/MC catalyst with respect to recycle run at 200 °C and 80 bar for 7 h.

Recycle run	Rhenium leaching (%) <sup>a</sup>	Ruthenium leaching (%) <sup>a</sup>
Fresh	1.01	0.28
1	0.96	0.40
2	1.47	0.74

<sup>a</sup> Determined by ICP-MS measurement.

200 °C and 80 bar for 7 h. Fresh and spent 0.3Re–0.3Ru/MC catalyst showed complete conversion of succinic acid, and selectivity and yield for BDO over the catalyst remained almost constant. Moreover, no significant metal leaching was observed (less than 2%) after each recycle test, as listed in Table 6. This implies that the strong interaction of Re–Ru metallic bond effectively suppressed leaching of metal species. Thus, 0.3Re–0.3Ru/MC catalyst served as a stable and reusable catalyst in the hydrogenation of succinic acid to BDO.

#### 4. Conclusion

A series of Re–Ru bimetallic catalysts supported on mesoporous carbon ((0.6 – x)Re–xRu/MC, x = 0, 0.15, 0.3, 0.45, and 0.6 mol%) were prepared by a single-step surfactant-templating method and a subsequent incipient wetness impregnation method, and they were used for liquid-phase hydrogenation of succinic acid to BDO. The effect of metal content on the catalytic activities and physicochemical properties of (0.6 – x)Re–xRu/MC was investigated. All the catalysts showed a well-developed mesoporous structure. It was found that a Re–Ru solid-solution phase was formed in the catalysts during the reduction process, facilitating the synergistic interaction between rhenium and ruthenium. It was also revealed that reducibility, metal dispersion, and oxidation state of (0.6 – x)Re–xRu/MC catalysts were strongly influenced by Re:Ru molar ratio. In particular, the ratios of Re<sup>0</sup>/Re<sub>total</sub> and Ru<sup>0</sup>/Ru<sub>total</sub> were closely related to the hydrogen adsorption behavior of the reduced (0.6 – x)Re–xRu/MC catalysts. The amount of weak hydrogen-binding sites of the catalysts increased with increasing Re<sup>0</sup>/Re<sub>total</sub> and Ru<sup>0</sup>/Ru<sub>total</sub> ratios. Catalytic performance in the hydrogenation of succinic acid to BDO over (0.6 – x)Re–xRu/MC showed a volcano-shaped trend with respect to Re:Ru molar ratio. TOF<sub>BDO</sub> increased with increasing the amount of weak hydrogen-binding sites of the reduced (0.6 – x)Re–xRu/MC catalysts. Among the catalysts tested, 0.3Re–0.3Ru/MC with the largest amount of weak hydrogen-binding sites showed the highest TOF<sub>BDO</sub>. Furthermore, 0.3Re–0.3Ru/MC served as a stable and reusable catalyst in the selective formation of BDO by hydrogenation of succinic acid.

#### Acknowledgement

This work was supported by the Global Frontier R&D Program on Center for Multiscale Energy System funded by the National Research Foundation under the Ministry of Education, Science and Technology, Korea (20110031575).

#### References

- [1] M.L. Morgan, Chem. Ind. 3 (1997) 166–168.
- [2] I. Bechthold, K. Bretz, S. Kabasci, R. Kopitzky, A. Springer, Chem. Eng. Technol. 31 (2008) 647–654.
- [3] C. Delhomme, D. Weuster-Botz, F.E. Kuhn, Green Chem. 11 (2009) 13–26.
- [4] A. Cukalovic, C.V. Stevens, Biofuels Bioprod. Bioref. 2 (2008) 505–529.
- [5] P. Gallezot, Chem. Soc. Rev. 41 (2012) 1538–1558.
- [6] T. Haas, B. Jaeger, R. Weber, S.F. Mitchell, C.F. King, Appl. Catal. A 280 (2005) 83–88.
- [7] S.-H. Chung, Y.-M. Park, M.-S. Kim, K.-Y. Lee, Catal. Today 185 (2012) 205–210.
- [8] B. Tapin, F. Epron, C. Espécel, B.K. Ly, C. Pinel, M. Besson, ACS Catal. 3 (2013) 2327–2335.
- [9] U.G. Hong, J. Lee, S. Hwang, I.K. Song, Catal. Lett. 141 (2011) 332–338.
- [10] R. Luque, J.H. Clark, K. Yoshida, P.L. Gai, Chem. Commun. 35 (2009) 5305–5307.
- [11] L. Rosi, M. Frediani, P. Frediani, J. Organomet. Chem. 695 (2010) 1314–1322.
- [12] U.G. Hong, J.K. Kim, J. Lee, J.K. Lee, J.H. Song, J. Yi, I.K. Song, Appl. Catal. A 469 (2014) 466–471.
- [13] U.G. Hong, H.W. Park, J. Lee, S. Hwang, J. Yi, I.K. Song, Appl. Catal. A 415 (2012) 141–148.
- [14] L. Corbel-Dimailly, B.-K. Ly, D.-P. Minh, B. Tapin, C. Espécel, F. Epron, A. Cabiac, E. Guillou, M. Besson, C. Pinel, ChemSusChem 6 (2013) 2388–2395.
- [15] D.P. Minh, M. Besson, C. Pinel, P. Fuertes, C. Petitjean, Top. Catal. 53 (2010) 1270–1273.
- [16] B.K. Ly, D.P. Minh, C. Pinel, M. Besson, B. Tapin, F. Epron, C. Espécel, Top. Catal. 55 (2012) 466–473.
- [17] R.V. Chaudhari, C.V. Rode, R.M. Deshpande, R. Jaganathan, T.M. Leib, P.L. Mills, Chem. Eng. Sci. 58 (2003) 627–632.
- [18] G. Beamson, A.J. Papworth, C. Phillips, A.M. Smith, R. Whyman, J. Catal. 278 (2011) 228–238.
- [19] V. Ponec, G.C. Bond, Stud. Surf. Sci. Catal. 95 (1993) 393–453.
- [20] T.B. Massalski, Binary Alloy Phase Diagrams, ASM International, Materials Park, 1990.
- [21] H.C. Yao, M. Shelef, J. Catal. 44 (1976) 392–403.
- [22] J. Okal, L. Kepinski, L. Krajczyk, M. Drozd, J. Catal. 188 (1999) 140–153.
- [23] I. Matos, S. Fernandes, L. Guerreiro, S. Barata, A.M. Ramos, J. Vital, I.M. Fonseca, Microporous Mesoporous Mater. 92 (2006) 38–46.
- [24] P. Arnoldy, E.M. Van-Oersa, O.S.L. Bruinsma, V.H.J. De-Beer, J.A. Moulijn, J. Catal. 93 (1985) 231–245.
- [25] P. Betancourt, A. Rives, R. Hubaut, C.E. Scott, J. Goldwaser, Appl. Catal. A 170 (1998) 307–314.
- [26] M. Bonarowska, A. Malinowski, Z. Karpinski, Appl. Catal. A 188 (1999) 145–154.
- [27] B.H. Isaacs, E.E. Petersen, J. Catal. 77 (1982) 43–52.
- [28] L. Ma, D. He, Top. Catal. 52 (2009) 834–844.
- [29] Y. Amada, Y. Shimi, S. Koso, T. Kubota, Y. Nakagawa, K. Tomishige, Appl. Catal. B 105 (2011) 117–127.
- [30] S.T. Homeyer, W.M.H. Sachtler, J. Catal. 118 (1989) 226–274.
- [31] K. Aika, K. Shimazaki, Y. Hattori, A. Ohya, S. Ohshima, K. Shiota, A. Ozaki, J. Catal. 92 (1985) 296–304.
- [32] P. Badenes, L. Daza, I. Rodriguez-Ramos, A. Guerrero-Ruiz, Stud. Surf. Sci. Catal. 112 (1997) 241–250.
- [33] Z.Q. Li, C.J. Lu, Z.P. Xia, Y. Zhou, Z. Luo, Carbon 45 (2007) 1686–1695.
- [34] Y. Zhu, W. Lu, H. Li, H. Wan, J. Catal. 246 (2007) 382–389.
- [35] Y. Yazawa, H. Yoshida, N. Takagi, S. Komai, A. Satsuma, T. Hattori, J. Catal. 187 (1999) 15–23.
- [36] Y. Yuan, T. Shido, Y. Iwasawa, Chem. Commun. 15 (2000) 1421–1422.
- [37] W.T. Tysoe, F. Zaera, G.A. Somorjai, Surf. Sci. 200 (1988) 1–14.
- [38] P.C.H. Mitchell, C.E. Scott, J.-P. Bonnelle, J.G. Grimblot, J. Catal. 107 (1987) 482–489.
- [39] S. Yagi, D. Kuni, Chem. Eng. Sci. 16 (1961) 372–379.
- [40] J.Y. Park, O. Levenspiel, Chem. Eng. Sci. 30 (1975) 1207–1214.
- [41] S.C. Su, J.N. Carstens, A.T. Bell, J. Catal. 176 (1998) 125–135.
- [42] P. Claus, Appl. Catal. A 291 (2005) 222–229.
- [43] J.-P. Tessonier, L. Pesant, G. Ehret, M.J. Ledoux, C. Pham-Huu, Appl. Catal. A 288 (2005) 203–210.
- [44] K. Baranowska, J. Okal, N. Miniajlik, Catal. Lett. 144 (2014) 447–459.
- [45] X. Dong, H.-B. Zhang, G.-D. Lin, Y.-Z. Yuan, K.R. Ysai, Catal. Lett. 85 (2003) 237–246.
- [46] C. Zupanc, A. Hornung, O. Hinrichsen, M. Muhler, J. Catal. 209 (2002) 501–514.
- [47] D.P. Vanderwiel, M. Pruski, T.S. King, J. Catal. 188 (1999) 186–202.